

An Effective Model of the Retinoic Acid Induced HL-60 Differentiation Program

Ryan Tasseff, Holly A. Jensen, Wei Dai, Rodica P. Bunaciu[†], Johanna Congleton[†], Andrew Yen[†], and Jeffrey D. Varner*

Robert Frederick Smith School of Chemical and Biomolecular Engineering and [†]Department of Biomedical Sciences, Cornell University, Ithaca NY 14853

Running Title: Effective modeling of HL-60 differentiation

To be submitted: *Frontiers in Systems Biology*

*Corresponding author:

Jeffrey D. Varner,

Professor, Robert Frederick Smith School of Chemical and Biomolecular Engineering,
244 Olin Hall, Cornell University, Ithaca NY, 14853

Email: jdv27@cornell.edu

Phone: (607) 255 - 4258

Fax: (607) 255 - 9166

Abstract

In this study, we present an effective model All-Trans Retinoic Acid (ATRA)-induced differentiation of HL-60 cells. The model describes a key architectural feature of ATRA-induced differentiation, positive feedback between an ATRA-inducible signalsome complex involving many proteins including Vav1, a guanine nucleotide exchange factor, and the activation of the mitogen activated protein kinase (MAPK) cascade. The model, which was developed by integrating logical rules with kinetic modeling, was significantly smaller than previous models. However, despite its simplicity, it captured key features of ATRA induced differentiation of HL-60 cells. We identified an ensemble of effective model parameters using measurements taken from ATRA-induced HL-60 cells. Using these parameters, model analysis predicted that MAPK activation was bistable as a function of ATRA exposure. Conformational experiments supported ATRA-induced bistability. These findings, combined with other literature evidence, suggest that positive feedback is central to a diversity of cell fate programs.

1 Introduction

2 Understanding the architecture of differentiation programs is an important therapeutic
3 challenge. Differentiation induction chemotherapy (DIC), using agents such as the vita-
4 min A derivative all-trans retinoic acid (ATRA), is a promising approach for the treatment
5 of many cancers (1–3). For example, ATRA treatment induces remission in 80–90% of
6 promyelocytic leukemia (APL) PML-RAR α -positive patients (4), thereby transforming a
7 fatal diagnosis into a manageable disease. However, remission is sometimes not durable
8 and relapsed cases exhibit emergent ATRA resistance (5, 6). To understand the basis of
9 this resistance, we must first understand the ATRA-induced differentiation program. To-
10 ward this challenge, lessons learned in model systems, such as the lineage-uncommitted
11 human myeloblastic cell line HL-60, could inform our analysis of the more complex dif-
12 ferentiation programs occurring in patients. Patient derived HL-60 leukemia cells have
13 been a durable experimental model since the 1970's to study differentiation (7). HL-60
14 undergoes cell cycle arrest and either myeloid or monocytic differentiation following stim-
15 ulation; ATRA induces G1/G0-arrest and myeloid differentiation in HL-60 cells, while 1,25-
16 dihydroxy vitamin D3 (D3) induces arrest and monocytic differentiation. Commitment to
17 cell cycle arrest and differentiation requires approximately 48 hr of treatment, during which
18 HL-60 cells undergo two division cycles.

19 Sustained mitogen-activated protein kinase (MAPK) activation is a defining feature of
20 ATRA-induced HL-60 differentiation. ATRA drives sustained MEK-dependent activation
21 of the Raf/MEK/ERK pathway, leading to arrest and differentiation (8). MEK inhibition re-
22 sults in the loss of ERK and Raf phosphorylation, and the failure to arrest and differentiate
23 (9). ATRA (and its metabolites) are ligands for the hormone activated nuclear transcrip-
24 tion factors retinoic acid receptor (RAR) and retinoid X receptor (RXR) (10). RAR/RXR
25 activation is necessary for ATRA-induced Raf phosphorylation (9), and the formation of
26 an ATRA-inducible signalsome complex at the membrane which drives MAPK activation

27 through a yet to be identified kinase activity. While the makeup of the signalsome com-
28 plex is not yet known, we do know that it is composed of Src family kinases Fgr and Lyn,
29 PI3K, c-Cbl, Slp76, and KSR, as well as IRF-1 transcription factors (11–15). Signalsome
30 formation and activity is driven by ATRA-induced expression of CD38 and the putative
31 heterotrimeric Gq protein-coupled receptor BLR1 (16, 17). BLR1, identified as an early
32 ATRA (or D3)-inducible gene using differential display (18), is necessary for MAPK ac-
33 tivation and differentiation (17), and is also involved with signalsome activity. Studies
34 of the BLR1 promoter identified a 5' 17bp GT box approximately 1 kb upstream of the
35 transcriptional start that conferred ATRA responsiveness (17). Members of the BLR1
36 transcriptional activator complex, e.g. NFATc3 and CREB, are phosphorylated by ERK,
37 JNK or p38 MAPK family members suggesting positive feedback between the signal-
38 some and MAPK activation (19). BLR1 overexpression enhanced Raf phosphorylation
39 and accelerated terminal differentiation, while Raf inhibition reduced BLR1 expression
40 and differentiation (20). BLR1 knock-out cells failed to activate Raf or differentiate in
41 the presence of ATRA (20). Interestingly, both the knockdown or inhibition of Raf, also
42 reduced BLR1 expression and functional differentiation (20). Thus, the expression of
43 signalsome components e.g., BLR1 was Raf dependent, while Raf activation depended
44 upon the siganlsome. A recent computational study of ATRA-induced differentiation in
45 HL-60 cells suggested that the BLR1-MAPK positive feedback circuit was sufficient to ex-
46 plain ATRA-induced sustained MAPK activation, and the expression of a limited number
47 of functional differentiation markers (21). Model analysis also suggested that Raf was the
48 most distinct of the MAPK proteins. However, this previous study developed and analyzed
49 a complex model, thus leaving open the critical question of what is the minimal positive
50 feedback circuit required to drive ATRA-induced differentiation.

51 In this study, we explored this question using a minimal mathematical model of the
52 key architectural feature of ATRA induced differentiation of HL-60 cells, namely positive

53 feedback between an ATRA-inducible signalsome complex and MAPK activation. The
54 ATRA responsive signalsome-MAPK circuit was then used to drive a downstream gene
55 expression program which encoded for the expression of functional differentiation mark-
56 ers. The effective model used a novel framework which integrated logical rules with ki-
57 netic modeling to describe gene expression and protein regulation, while largely relying
58 upon biophysical parameters from the literature. This formulation significantly reduced
59 the size and complexity of the model compared to the previous study of Tasseff et al.,
60 while increasing the breadth of the biology described (21). The effective model, despite
61 its simplicity, captured key features of ATRA induced differentiation of HL-60 cells. Model
62 analysis predicted the bistability of MAPK activation as a function of ATRA exposure; con-
63 formational experiments supported ATRA-induced bistability. Model simulations were also
64 consistent with measurements of the influence of MAPK inhibitors, and the failure of BLR1
65 knockout cells to differentiate when exposed to ATRA. Lastly, we showed by through im-
66 munoprecipitation studies, that the guanine nucleotide exchange factor Vav1 is potentially
67 a new ATRA-inducible member of the siganlsome complex. Taken together, these findings
68 when combined with other literature evidence, suggested that positive feedback architec-
69 tures are central to differentiation programs generally, and necessary for ATRA-induced
70 differentiation.

71 **Results**

72 We constructed an effective model of ATRA-induced HL-60 differentiation which described
73 signaling and gene expression events following the addition of ATRA (Fig. 1). The model
74 connectivity was developed from literature and the studies presented here (Table ZZ). We
75 decomposed the ATRA program into three modules; a signal initiation module that sensed
76 and transformed the ATRA signal into activated cRaf-S621 and the ATRA-RXR/RAR (Trig-
77 ger) signals (Fig. 1A); a signal integration module that controlled the expression of up-
78 stream transcription factors given cRaf-S621 and activated Trigger signals (Fig. 1B); and
79 a phenotype module which encoded the expression of functional differentiation markers
80 from the ATRA-inducible transcription factors (Fig. 1C). Each component of these mod-
81 ules was described by a mRNA and protein balance equation. Additionally, the signal
82 initiation module also described the abundance of activated species e.g., Trigger and
83 cRaf-S621 whose values were derived from unactivated Trigger and cRaf protein levels.
84 Lastly, because the population of HL-60 cells was dividing (at least before ATRA-induced
85 cell cycle arrest), we also considered a dilution term in all balance equations. The sig-
86 nal initiation module contained nine differential equations, while the signal integration and
87 phenotype modules were collectively encoded by 54 differential equations. Model pa-
88 rameters were taken literature, or estimated from experimental data taken from literature
89 using heuristic optimization (see materials and methods).

90 The signal initiation module recapitulated sustained signalsome/MAPK activation fol-
91 lowing exposure to $1\mu\text{M}$ ATRA (Fig. 2A-B). An ensemble of effective model parameters
92 was estimated by minimizing the difference between simulations and time-series mea-
93 surements of BLR1 mRNA and cRaf-S621 following the addition of $1\mu\text{M}$ ATRA. We fo-
94 cused on the S621 phosphorylation site of cRaf since enhanced phosphorylation at this
95 site is a defining characteristic of sustained MAPK activation in HL-60. The effective
96 model captured both ATRA-induced BLR1 expression (Fig. 2A) and sustained phospho-

97 phosphorylation of cRaf-pS621 (Fig. 2B) in a growing population of HL-60 cells. However, the
98 effective model failed to capture the decline of BLR1 message after 48 hr of ATRA expo-
99 sure. Next, we tested the response of the signalsome/MAPK signaling module to different
100 ATRA dosages.

101 The signalsome/MAPK signaling model was bistable with respect to ATRA induction
102 (Fig. 2C-D). Nullcline analysis predicted two stable steady-states and a single unstable
103 state when ATRA was present below a critical threshold (Fig. 2C). In the lower stable
104 state, neither the signalsome nor cRaf-pS621 were present (thus, the differentiation pro-
105 gram was deactivated). However, at the high stable state, both the signalsome and cRaf-
106 pS621 were present, allowing for sustained activation and differentiation. Interestingly,
107 when ATRA was above a critical threshold, only the activated state was accessible (Fig.
108 2D). To test these findings, we first identified the ATRA threshold. We exposed HL-60 cells
109 to different ATRA concentrations for 72 hr (Fig. 2E). Morphological changes associated
110 with differentiation were visible for ATRA $\geq 0.25 \mu\text{M}$, suggesting the critical ATRA thresh-
111 old was near this concentration. Next, we conducted washout ATRA washout experiments
112 to determine if activated cells remained activated even in the absence of ATRA. HL-60
113 cells locked into an activated state remained activated following ATRA withdraw (Fig. 3).
114 Sustained activation resulted from reinforcing feedback between the signalsome and the
115 MAPK pathway. Thus, following activation, if we inhibited or removed elements from the
116 effective circuit we expected the signalsome and MAPK signals to decay. We simulated
117 ATRA induced activation in the presence of kinase inhibitors, and without key circuit ele-
118 ments. Consistent with experimental results using multiple MAPK inhibitors, ATRA activa-
119 tion in the presence of MAPK inhibitors lowered the steady-state value of signalsome (Fig.
120 3A). In the presence of BLR1, the signalsome and cRaf-pS621 signals were maintained
121 following ATRA withdraw (Fig. 3B, blue). On the other hand, BLR1 deletion removed
122 the ability of the circuit to maintain a sustained MAPK response following the withdraw

123 of ATRA (Fig. 3B, gray). Lastly, washout experiments in which cells were exposed to
124 1 μ M ATRA for 24 hr, and then transferred to fresh media without ATRA, confirmed the
125 persistence of the self sustaining activated state for up to 144 hr (Fig. 3C). Thus, these
126 experiments and simulations confirmed that reinforcing positive feedback likely drives the
127 ATRA-induced differentiation program. Next, we analyzed the ATRA-induced downstream
128 gene expression program following signalsome and cRaf activation.

129 The reduced order gene expression model described signal integration and ATRA-
130 induced gene expression events in wild-type HL-60 cells (Fig. 4). The signalsome-MAPK
131 model produced two outputs, Trigger and cRaf-S621 which drove the downstream dif-
132 ferentiation program. In particular, Trigger, which is a surrogate for the RAR α /RXR tran-
133 scriptional complex, regulated the expression of the transcription factors CCATT/enhancer
134 binding protein α (C/EBP α), PU.1, and EGR1. In turn, these transcription factors, in com-
135 bination with cRaf-S621, regulated the expression of downstream phenotypic markers
136 such as CD38, CD11b or P47Phox. We assembled the connectivity of the signal integra-
137 tion program driven by Trigger, and the phenotypic program from literature (supplemental
138 materials). We estimated the parameters of the signal integration and phenotype pro-
139 grams from previous studies which contained both steady-state and dynamic measure-
140 ments of transcription factor and phenotypic marker expression following the addition of
141 ATRA [REFHERE]. The model simulations captured the time dependent expression of
142 both CD38 and CD11b following the addition ATRA (Fig. 4A), and steady-state values for
143 upstream members of the signal integration unit (Fig. 4B).

144 The composition of the siganlsome, and the kinase ultimately responsible for medi-
145 ating ATRA-induced Raf activation is currently unknown. To explore this question, we
146 conducted immunoprecipitation and subsequent Western blotting to identify physical in-
147 teractions between Raf and 19 putative interaction partners. A panel of 19 possible Raf
148 interaction partners (kinases, GTPases, scaffolding proteins etc) was constructed based

upon known signaling pathways. We did not consider the most likely binding partner, the small GTPase RAS, as previous studies have ruled it out in MAPK activation in HL-60 cells (20, 22). Total Raf was used as a bait protein for the immunoprecipitation studies. Interrogation of the Raf interactome suggested Vav1 was involved with ATRA-induced initiation of MAPK activity (Fig. 5). Western blot analysis using total Raf and pS621 Raf specific antibodies confirmed the presence of the bait protein, total and phosphorylated forms, in the immunoprecipitate (Fig. 5A). Of the 19 proteins sampled, Vav1, Src, CK2, Akt, and 14-3-3 precipitated with Raf, suggesting a direct physical interaction was possible. However, only the associations between Raf and Vav1 and Raf and Src were ATRA-inducible (Fig. 5). Furthermore, the Vav1 and Src associations were correlated with pS621 Raf abundance in the precipitate. Others proteins e.g., CK2, Akt and 14-3-3, generally bound Raf regardless of phosphorylation status or ATRA treatment. The remaining 14 proteins were expressed in whole cell lysate (Fig. 5B), but were not detectable in the precipitate of Raf IP. Treatment with the Raf kinase inhibitor GW5074 following ATRA exposure reduced the association of both Vav1 with Raf and Src with Raf (Fig. 5), although the signal intensity for Src was notably weak. However, GW5074 did not influence the association of CK2 or 14-3-3 with Raf, further demonstrating their independence from Raf phosphorylation. Interestingly, the Raf-Akt interaction qualitatively increased following treatment with GW5074; however, it remained unaffected by treatment with ATRA. Src family kinases are known to be important in myeloid differentiation (23) and their role in HL-60 differentiation has been investigated elsewhere (11). Given the existing work and variable reproducibility in the context of the Raf immunoprecipitate, we did not investigate the role of Src further in this study. Taken together, the immunoprecipitation and GW5074 results implicated Vav1 association to be correlated with Raf activation following ATRA-treatment. Previous studies demonstrated that a Vav1-Slp76-Cbl-CD38 complex plays an important role in ATRA-induced MAPK activation and differentiation of HL-60 cells (13). Here we

¹⁷⁵ did not observe direct interaction of Raf with Cbl or Slp76; however, this complex could
¹⁷⁶ be involved upstream.

¹⁷⁷ Next, we considered the effect of the Raf kinase inhibitor GW5074 on functional mark-
¹⁷⁸ ers of ATRA-induced growth arrest and differentiation. Inhibition of Raf kinase activity
¹⁷⁹ modulated MAPK activation and differentiation markers following ATRA exposure (Fig.
¹⁸⁰ 5D-F). ATRA treatment alone statistically significantly increased the G1/G0 percentage
¹⁸¹ over the untreated control, while GW5074 alone had a negligible effect on the cell cycle
¹⁸² distribution (Fig. 5D). Surprisingly, the combination of GW5074 and ATRA statistically
¹⁸³ significantly increased the G1/G0 population ($82 \pm 1\%$) compared with ATRA alone (61
¹⁸⁴ $\pm 0.5\%$). Increased G1/G0 arrest following the combined treatment with GW5074 and
¹⁸⁵ ATRA was unexpected, as the combination of ATRA and the MEK inhibitor (PD98059) has
¹⁸⁶ been shown previously to decrease ATRA-induced growth arrest (8). However, growth ar-
¹⁸⁷ rest is not the sole indication of functional differentiation. Expression of the cell surface
¹⁸⁸ marker CD11b has also been shown to coincide with HL-60 cells myeloid differentiation
¹⁸⁹ (24). We measured CD11b expression, for the various treatment groups, using immuno-
¹⁹⁰ fluorescence flow cytometry 48 hr post-treatment. As with G1/G0 arrest, ATRA alone
¹⁹¹ increased CD11b expression over the untreated control, while GW5074 further enhanced
¹⁹² ATRA-induced CD11b expression (Fig. 5E). GW5074 alone had no statistically significant
¹⁹³ effect on CD11b expression, compared with the untreated control. Lastly, the inducible re-
¹⁹⁴ active oxygen species (ROS) response was used as a functional marker of differentiated
¹⁹⁵ neutrophils (16). We measured the ROS response induced by the phorbol ester 12-O-
¹⁹⁶ tetradecanoylphorbol-13-acetate (TPA) using flow cytometry. Untreated cells showed no
¹⁹⁷ discernible TPA response, with only $7.0 \pm 3.0\%$ ROS induction (Fig. 5F). Cells treated
¹⁹⁸ with ATRA had a significantly increased TPA response, $53 \pm 7\%$ ROS induction 48 hr
¹⁹⁹ post-treatment. Treatment with both ATRA and GW5074 statistically significantly reduced
²⁰⁰ ROS induction ($22 \pm 0.6\%$) compared to ATRA alone. Interestingly, Western blot analy-

201 sis did not detect a GW5074 effect on ATRA-induced expression of p47phox, a required
202 upstream component of the ROS response (Fig. 5F, bottom). Thus, the inhibitory effect
203 of GW5074 on inducible ROS might occur downstream of p47phox expression. How-
204 ever, the ROS producing complex is MAPK dependent, therefore it is also possible that
205 GW5074 inhibited ROS production by interfering with MAPK activation (in which case the
206 p47Phox marker might not accurately reflect phenotypic conversion and differentiation).

207 **Discussion**

208 In this study, we presented an effective model of ATRA-inducible differentiation of HL-60
209 cells which encoded positive feedback between the ATRA-inducible signalsome complex
210 and the MAPK pathway. Despite its simplicity, the model captured key features of the
211 ATRA induced differentiation such as sustained MAPK activation, and bistability with re-
212 spect to ATRA exposure. We also reported a new ATRA-inducible component of the
213 signalsome, Vav1. Vav1 is a guanine nucleotide exchange factor for Rho family GTPases
214 that activate pathways leading to actin cytoskeletal rearrangements and transcriptional al-
215 terations (25). The Vav1/Raf association correlated with Raf activity, was ATRA-inducible
216 and decreased after treatment with GW5074. The presence of Vav1 in Raf/Grb2 com-
217 plexes has been shown to correlate with increased Raf activity in mast cells (26). Fur-
218 thermore, studies on Vav1 knockout mice demonstrated that the loss of Vav1 resulted
219 in deficiencies of ERK signaling for both T-cells as well as neutrophils (27, 28). While its
220 function in the signalsome is unclear, Vav1 has been shown to associate with a Cbl-Slp76-
221 CD38 complex in an ATRA-dependent manner; furthermore, transfection of HL-60 cells
222 with Cbl mutants that fail to bind CD38, yet still bind Slp76 and Vav1, prevented ATRA-
223 induced MAPK activation (13). Thus, interaction of Cbl-Slp76-Vav1 and CD38 appears to
224 be required for transmission of the ATRA signal by the signalsome.

225 We conducted immunoprecipitation studies and identified a limited number of ATRA-
226 dependent and -independent Raf interaction partners. While we were unable to detect
227 the association of Raf with common kinases and GTPases such as PKC, PKA, p38, Rac
228 and Rho, we did establish potential interactions between Raf and key partners such as
229 Vav1, Src, Akt, CK2 and 14-3-3. All of these partners are known to be associated with Raf
230 activation or function. Src is known to bind Raf through an SH2 domain, and this associ-
231 ation has been shown to be dependent of the serine phosphorylation of Raf (29). Thus,
232 an ATRA inducible Src/Raf association may be a result of ATRA-induced Raf phospho-

233 phosphorylation at S259 or S621. We also identified an interaction between Raf and the Ser/Thr
234 kinases Akt and CK2. Akt can phosphorylate Raf at S259, as demonstrated by studies
235 in a human breast cancer line (30). CK2 can also phosphorylate Raf, although the lit-
236 erature has traditionally focused on S338 and not S621 or S259(31). However, neither
237 of these kinase interactions were ATRA-inducible, suggesting their association with Raf
238 alone was not associated with ATRA-induced Raf phosphorylation. The adapter protein
239 14-3-3 was also constitutively associated with Raf. The interaction between Raf and 14-
240 3-3 has been associated with both S621 and S259 phosphorylation and activity (32).
241 Additionally, the association of Raf with 14-3-3 not only stabilized S621 phosphorylation,
242 but also reversed the S621 phosphorylation from inhibitory to activating (33). Finally, we
243 found that Vav1/Raf association correlated with Raf activity, was ATRA-inducible and de-
244 creased after treatment with GW5074. The presence of Vav1 in Raf/Grb2 complexes has
245 been shown to correlate with increased Raf activity in mast cells (26). Furthermore, stud-
246 ies on Vav1 knockout mice demonstrated that the loss of Vav1 resulted in deficiencies of
247 ERK signaling for both T-cells as well as neutrophils (27, 28). Interestingly, while an in-
248 tegrin ligand-induced ROS response was blocked in Vav1 knockout neutrophils, TPA was
249 able to bypass the Vav1 requirement and stimulate both ERK phosphorylation and ROS
250 induction (28). In this study, the TPA-induced ROS response was dependent upon Raf
251 kinase activity, and was mitigated by the addition of GW5074. It is possible that Vav1 is
252 downstream of various integrin receptors but upstream of Raf in terms of inducible ROS
253 responses. Vav1 has also been shown to associate with a Cbl-Slp76-CD38 complex in an
254 ATRA-dependent manner; furthermore, transfection of HL-60 cells with Cbl mutants that
255 fail to bind CD38, yet still bind Slp76 and Vav1, prevents ATRA-induced MAPK activation
256 (13). The literature suggest a variety of possible receptor-signaling pathways, which in-
257 volve Vav1, for MAPK activation; moreover, given the ATRA-inducible association Vav1
258 may play a direct role in Raf activation.

259 We hypothesized that Vav1 is a member of an ATRA-inducible complex which propels
260 sustained MAPK activation, arrest and differentiation. Initially, ATRA-induced Vav1 ex-
261 pression drives increased association between Vav1 and Raf. This increased interaction
262 facilitates phosphorylation and activation of Raf by pre-bound Akt and/or CK2 at S621
263 or perhaps S259. Constitutively bound 14-3-3 may also stabilize the S621 phosphory-
264 lation, modulate the activity and/or up-regulate autophosphorylation. Activated Raf can
265 then drive ERK activation, which in turn closes the positive feedback loop by activating
266 Raf transcription factors, e.g. Sp1 and/or STAT1 (34–37). We tested this working hy-
267 pothesis using mathematical modeling. The model recapitulated both ATRA time-course
268 data as well as the GW5074 inhibitor effects. This suggested the proposed Raf-Vav1
269 architecture was at least consistent with the experimental studies. Further, analysis of
270 the Raf-Vav1 model identified bistability in ppERK levels. Thus, two possible MAPK ac-
271 tivation branches were possible for experimentally testable ATRA values. The analysis
272 also suggested the ATRA-induced Raf-Vav1 architecture could be locked into a sustained
273 signaling mode (high ppERK) even in the absence of a ATRA signal. This locked-in prop-
274 erty could give rise to an ATRA-induction memory. We validated the treatment memory
275 property predicted by the Raf-Vav1 circuit experimentally using ATRA-washout experi-
276 ments. ERK phosphorylation levels remained high for more then 96 hr after ATRA was
277 removed. Previous studies demonstrated that HL-60 cells possessed an inheritable mem-
278 ory of ATRA stimulus (38). Although the active state was self-sustaining, the inactive state
279 demonstrated considerable robustness to perturbation. For example, we found that 50x
280 overexpression of Raf was required to reliably lock MAPK into the activated state, while
281 small perturbations had almost no effect on ppERK levels over the entire ensemble. CD38
282 expression correlated with the ppERK, suggesting its involvement in the signaling com-
283 plex. Our computational and experimental results showed that positive feedback, through
284 ERK-dependent Raf expression, could sustain MAPK signaling through many division cy-

285 cles. Such molecular mechanisms could underly aspects of cellular memory associated
286 to consecutive ATRA treatments.

287 Several engineered, or naturally occurring systems involved in cell fate decisions incor-
288 porate positive feedback and bistability (39). One of the most well studied cell fate circuits
289 is the Mos mitogen-activated protein kinase cascade in *Xenopus* oocytes. This cascade
290 is activated when oocytes are induced by the steroid hormone progesterone (40). The
291 MEK-dependent activation of p42 MAPK stimulates the accumulation of the Mos onco-
292 protein, which in turn activates MEK, thereby closing the feedback loop. This is similar to
293 the differentiation circuit presented here; ATRA drives signalsome which activates MAPK,
294 cell-cycle arrest, differentiation and signalsome. Thus, while HL-60 and *Xenopus* oocytes
295 are vastly different biological models, they share similar cell fate decision architectures.
296 Other unrelated cell fate decisions such as programmed cell death have also been sug-
297 gested to be bistable (41). Still more biochemical networks important to human health,
298 for example the human coagulation or complement cascades, also feature strong positive
299 feedback elements (42). Thus, while positive feedback is sometimes not desirable in man-
300 made systems, it may be at the core of a diverse variety of cell fate programs and other
301 networks important to human health.

302 Model performance was impressive given its limited size. However, there were several
303 issues to explore further. First, there was likely missing connectivity in the effective differ-
304 entiation circuit. Decreasing BLR1 expression with simultaneously sustained cRaf-pS261
305 activation was not captured by the current network architecture. This suggested that
306 signalsome, once activated, had a long lifetime as decreased BLR1 expression did not
307 impact cRaf-pS261 abundance. We could model this by separating signalsome formation
308 into an inactive precursor pool that is transformed to a long-lived activated signalsome by
309 MAPK activation. We should also explore adding additional downstream biological mod-
310 ules to this skeleton model, for example the upregulation of reactive oxygen markers such

311 as p47Phox or cell cycle arrest components to capture the switch from an actively prolif-
312 erating population to a population in G0-arrest. Next, the choice of max/min integration
313 rules or the particular form of the transfer functions could also be explored. Integration
314 rules other than max/min could be used, such as the mean or the product, assuming the
315 range of the transfer functions is always $f \in [0, 1]$. Alternative integration rules might
316 have different properties which could influence model identification or performance. For
317 example, a mean integration rule would be differentiable, allowing derivative-based opti-
318 mization approaches to be used. The form of the transfer function could also be explored.
319 We choose hill-like functions because of their prominence in the systems and synthetic
320 biology community. However, many other transfer functions are possible.

321 **Materials and Methods**

322 *Effective ATRA differentiation model.* ATRA induced signaling events were modeled us-
 323 ing saturation kinetics within an ordinary differential equation (ODE) framework:

$$\frac{1}{\tau_i} \frac{dx_i}{dt} = \sum_{j=1}^{\mathcal{R}} \sigma_{ij} r_j(\mathbf{x}, \epsilon, \mathbf{k}) - (\mu + k_d) x_i \quad i = 1, 2, \dots, \mathcal{M} \quad (1)$$

324 The quantity x_i denotes concentration of signaling species i , while \mathcal{R} and \mathcal{M} denote the
 325 number of signaling reactions and signaling species in the model, respectively. The quan-
 326 tity τ_i denotes a time scale parameter for species i which captures un-modeled effects; in
 327 the current study $\tau_i = 1$ for all species. The quantity $r_j(\mathbf{x}, \epsilon, \mathbf{k})$ denotes the rate of pro-
 328 cess j . Typically, process j is a non-linear function of biochemical and enzyme species
 329 abundance, as well as unknown model parameters \mathbf{k} ($\mathcal{K} \times 1$). The quantity σ_{ij} denotes the
 330 stoichiometric coefficient for species i in reaction j . If $\sigma_{ij} > 0$, species i is produced by
 331 reaction j . Conversely, if $\sigma_{ij} < 0$, species i is consumed by reaction j , while $\sigma_{ij} = 0$ indi-
 332 cates species i is not connected with reaction j . Lastly, μ denotes the specific growth rate,
 333 and k_d denotes the rate constant controlling cell death. Species balances were subject to
 334 the initial conditions $\mathbf{x}(t_o) = \mathbf{x}_o$.

335 Signaling rate processes were written as the product of a kinetic term (\bar{r}_j) and a control
 336 term (v_j) in the HL-60 model. The rate of an enzyme catalyzed process was modeled
 337 using saturation kinetics:

$$\bar{r}_j = k_j \epsilon_i \prod_{s \in m_j^-} \left(\frac{x_s}{K_{js} + x_s} \right) \quad (2)$$

338 where k_j denotes the catalytic rate constant for reaction j , ϵ_i denotes the abundance of the
 339 enzyme catalyzing reaction j , and K_{js} denotes the saturation constant for species s and
 340 $s \in m_j$ denotes the set of *reactants* for reaction j . The control terms $0 \leq v_j \leq 1$ depended
 341 upon the combination of factors which influenced rate process j . For each rate, we used

342 a rule-based approach to select from competing control factors. If rate j was influenced
 343 by $1, \dots, m$ factors, we modeled this relationship as $v_j = \mathcal{I}_j(f_{1j}(\cdot), \dots, f_{mj}(\cdot))$ where
 344 $0 \leq f_{ij}(\cdot) \leq 1$ denotes a regulatory transfer function quantifying the influence of factor i
 345 on rate j . The function $\mathcal{I}_j(\cdot)$ is an integration rule which maps the output of regulatory
 346 transfer functions into a control variable. In this study, we used $\mathcal{I}_j \in \{\min, \max\}$ and hill
 347 transfer functions (43). If a process had no modifying factors, $v_j = 1$.

348 The HL-60 model described both signal transduction and gene expression events fol-
 349 lowing the addition of ATRA. The output of the signal transduction model was the input to
 350 the gene expression model. For each gene $j = 1, 2, \dots, \mathcal{G}$, we modeled both the mRNA
 351 (m_j) and protein (p_j):

$$\frac{dm_j}{dt} = r_{T,j} - (\mu + \theta_{m,j}) m_j + \lambda_j \quad (3)$$

$$\frac{dp_j}{dt} = r_{X,j} - (\mu + \theta_{p,j}) p_j \quad (4)$$

352 The terms $r_{T,j}$ and $r_{X,j}$ denote the specific rates of transcription, and translation while
 353 the terms $\theta_{m,j}$ and $\theta_{p,j}$ denote first-order degradation constants for mRNA and protein,
 354 respectively. The specific transcription rate was modeled as the product of a kinetic term
 355 $\bar{r}_{T,j}$ and a control term u_j which described how the abundance of transcription factors, or
 356 other regulators influenced the expression of gene j . The kinetic rate of transcription was
 357 modeled as:

$$\bar{r}_{T,j} = V_T^{\max} \left(\frac{L_{T,o}}{L_{T,j}} \right) \left(\frac{G_j}{K_T + G_j} \right) \quad (5)$$

358 where the maximum gene expression rate V_T^{\max} was defined as the product of a char-
 359 acteristic transcription rate constant (k_T) and the abundance of RNA polymerase (R_1),
 360 $V_T^{\max} = k_T (R_1)$. The $(L_{T,o}/L_{T,j})$ term denotes the ratio of transcription read lengths,
 361 where $L_{T,o}$ is a characteristic gene length, and $L_{T,j}$ denotes the length of gene j . Thus,
 362 the $(L_{T,o}/L_{T,j})$ term is gene specific correction to the characteristic transcription rate. The

363 degradation rate constants were defined as $\theta_{m,j}$ and $\theta_{p,j}$ denote characteristic degradation
 364 constants for mRNA and protein, respectively.

365 The gene expression control term $0 \leq u_j \leq 1$ depended upon the combination of
 366 factors which influenced rate process j . If the expression of gene j was influenced
 367 by $1, \dots, m$ factors, we modeled this relationship as $u_j = \mathcal{I}_j(f_{1j}(\cdot), \dots, f_{mj}(\cdot))$ where
 368 $0 \leq f_{ij}(\cdot) \leq 1$ denotes a regulatory transfer function quantifying the influence of factor
 369 i on the expression of gene j , and $\mathcal{I}_j(\cdot)$ denotes an integration rule. In this study, the
 370 integration rule governing gene expression was the weighted fraction of promoter config-
 371 urations resulting in gene expression. Thus, the control variable u_j took the form:

$$u_j = \frac{W_{R_{1,j}} + \sum_n W_{nj} f_{nj}}{1 + W_{R_{1,j}} + \sum_d W_{dj} f_{dj}} \quad (6)$$

372 where the numerator, the weighted sum (with weights W_{nj}) of promoter configurations
 373 leading to gene expression, was normalized by all possible promoter configurations. The
 374 likelihood of each configuration was quantified by the transfer function f_{nj} (which we mod-
 375 eled using hill like functions), while the lead term in the numerator $W_{R_{1,j}}$ denotes the
 376 weight of constitutive expression for gene j . If a gene expression process had no modify-
 377 ing factors, $u_j = 1$. Lastly, the specific translation rate was modeled as:

$$r_{X,j} = V_X^{\max} \left(\frac{m_j}{K_X + m_j} \right) \quad (7)$$

378 where V_X^{\max} denotes a characteristic maximum translation rate estimated from literature,
 379 and K_X denotes a translation saturation constant. The characteristic maximum translation
 380 rate was defined as the product of a characteristic translation rate constant (k_X) and the
 381 Ribosome abundance (R_2), $V_X^{\max} = k_X (R_2)$.

382 In this study, we estimated the W_{ij} parameters, and the parameters in the trans-

383 fer functions f_{dj} from gene expression data sets. On the other hand, we estimated
 384 $k_T, k_X, \theta_{m,j}, \theta_{p,j}, R_1$ and R_2 using estimates of transcription and translation rates, the half-
 385 life of a typical mRNA and protein, and a typical value for the copies per cell of RNA
 386 polymerase and ribosomes from literature (44). The saturation constants K_X and K_T
 387 were adjusted so that gene expression and translation resulted in gene products on a bio-
 388 logically realistic concentration scale. Lastly, we calculated the concentration for gene G_j
 389 by assuming, on average, that a cell had two copies of each gene at any given time. Thus,
 390 the bulk of our gene expression parameters were based directly upon literature values,
 391 and were not adjusted during model identification. The values used for the characteris-
 392 tic transcription/translation parameters, degradation constants and macromolecular copy
 393 number are given in the supplemental materials along with the specific formulas required
 394 to calculate all derived constants.

395 *Estimation of signaling and gene expression model parameters.* Signal and gene ex-
 396 pression model parameters were estimated by minimizing the squared difference between
 397 simulations and experimental data set j :

$$E_j(\mathbf{k}) = \sum_{i=1}^{\mathcal{T}_j} \left(\hat{\mathcal{M}}_{ij} - \hat{y}_{ij}(\mathbf{k}) \right)^2 + \left(\frac{\mathcal{M}'_{ij} - \max y_{ij}}{\mathcal{M}'_{ij}} \right)^2 \quad (8)$$

398 The terms $\hat{\mathcal{M}}_{ij}$ and \hat{y}_{ij} denote scaled experimental observations and simulation outputs
 399 at time i from training set j , where \mathcal{T}_j denoted the number of time points for data set j .
 400 The first term in Eqn. (8) quantified the relative simulation error. We used immunoblot
 401 intensity measurements for model training. Thus, we trained the model on the *relative*
 402 change between bands within each data set. Suppose we have the intensity of species x
 403 at time $\{t_1, t_2, \dots, t_n\}$ in condition j . The scaled value $0 \leq \hat{\mathcal{M}}_{ij} \leq 1$ is given by:

$$\hat{\mathcal{M}}_{ij} = \left(\mathcal{M}_{ij} - \min_i \mathcal{M}_{ij} \right) / \left(\max_i \mathcal{M}_{ij} - \min_i \mathcal{M}_{ij} \right) \quad (9)$$

404 where $\hat{M}_{ij} = 0$ and $\hat{M}_{ij} = 1$ describe the lowest (highest) intensity bands. A similar
405 scaling was used for the simulation output. The second term in the objective function
406 ensured a realistic concentration scale was estimated by the model. We set the highest
407 intensity band to $M'_{ij} = 10$ [AU] for all simulations. We minimized the total model residual
408 $\sum_j E_j$ using heuristic optimization starting from a random initial parameter guess.

409 The signaling and gene expression model equations were implemented in Julia and
410 solved using the CVODE routine of the Sundials package (45, 46). The model code and
411 parameter ensemble is freely available under an MIT software license and can be down-
412 loaded from <http://www.varnerlab.org>.

413 *Cell culture and treatment* Human myeloblastic leukemia cells (HL-60 cells) were grown
414 in a humidified atmosphere of 5% CO₂ at 37°C and maintained in RPMI 1640 from Gibco
415 (Carlsbad, CA) supplemented with 5% heat inactivated fetal bovine serum from Hyclone
416 (Logan, UT) and 1× antibiotic/antimicotic (Gibco, Carlsbad, CA). Cells were cultured in
417 constant exponential growth (47). Experimental cultures were initiated at 0.1×10^6 cells/mL
418 24 hr prior to ATRA treatment; if indicated, cells were also treated with GW5074 (2 μ M) 18
419 hr before ATRA treatment. For the cell culture washout experiments, cells were treated
420 with ATRA for 24 hr, washed 3x with prewarmed serum supplemented culture medium
421 to remove ATRA, and reseeded in ATRA-free media as described. Western blot analysis
422 was performed at incremental time points after removal of ATRA.

423 *Chemicals* All-Trans Retinoic Acid (ATRA) from Sigma-Aldrich (St. Louis, MO) was dis-
424 solved in 100% ethanol with a stock concentration of 5mM, and used at a final concen-
425 tration of 1 μ M (unless otherwise noted). The cRaf inhibitor GW5074 from Sigma-Aldrich
426 (St. Louis, MO) was dissolved in DMSO with a stock concentration of 10mM, and used
427 at a final concentration of 2 μ M. HL-60 cells were treated with 2 μ M GW5074 with or with-
428 out ATRA (1 μ M) at 0 hr. This GW5074 dosage had a negligible effect on the cell cycle
429 distribution, compared to ATRA treatment alone.

430 *Immunoprecipitation and western blotting* Approximately 1.2×10^7 cells were lysed using
431 $400\mu\text{L}$ of M-Per lysis buffer from Thermo Scientific (Waltham, MA). Lysates were cleared
432 by centrifugation at $16,950 \times g$ in a micro-centrifuge for 20 min at 4°C . Lysates were
433 pre-cleared using $100\mu\text{L}$ protein A/G Plus agarose beads from Santa Cruz Biotechnology
434 (Santa Cruz, CA) by inverting overnight at 4°C . Beads were cleared by centrifugation and
435 total protein concentration was determined by a BCA assay (Thermo Scientific, Waltham,
436 MA). Immunoprecipitations were setup by bringing lysate to a concentration of 1g/L in a
437 total volume of $300\mu\text{L}$ (M-Per buffer was used for dilution). The anti-Raf antibody was
438 added at $3\mu\text{L}$. A negative control with no bait protein was also used to exclude the di-
439 rect interaction of proteins with the A/G beads. After 1 hr of inversion at 4°C , $20\mu\text{L}$ of
440 agarose beads was added and samples were left to invert overnight at 4°C . Samples
441 were then washed three times with M-Per buffer by centrifugation. Finally proteins were
442 eluted from agarose beads using a laemmli loading buffer. Eluted proteins were resolved
443 by SDS-PAGE and Western blotting. Total lysate samples were normalized by total protein
444 concentration ($20\mu\text{g}$ per sample) and resolved by SDS-PAGE and Western blotting. Sec-
445 ondary HRP bound antibody was used for visualization. All antibodies were purchased
446 from Cell Signaling (Boston, MA) with the exception of α -p621 Raf which was purchased
447 from Biosource/Invitrogen (Carlsbad, CA), and α -CK2 from BD Biosciences (San Jose,
448 CA).

449 *Morphology assessment* Untreated and ATRA-treated HL-60 cells were collected after
450 72 hr and cytocentrifuged for 3 min at 700 rpm onto glass slides. Slides were air-dried
451 and stained with Wright's stain. Slide images were captured at 40X (Leica DM LB 100T
452 microscope, Leica Microsystems).

453 **Competing interests**

454 The authors declare that they have no competing interests.

455 **Author's contributions**

456 J.V and A.Y directed the study. R.T, H.J and J.C conducted the cell culture measure-
457 ments. J.V and W.D developed the reduced order HL-60 models and the parameter en-
458 semble. W.D analyzed the model ensemble, and generated figures for the manuscript.
459 The manuscript was prepared and edited for publication by W.D, A.Y and J.V.

460 **Acknowledgements**

461 We gratefully acknowledge the suggestions from the anonymous reviewers to improve
462 this manuscript.

463 **Funding**

464 We acknowledge the financial support to J.V. by the National Science Foundation CA-
465 REER (CBET-0846876) for the support of R.T. and H.J. In addition, we acknowledge
466 support to A.Y. from the National Institutes of Health (CA 30555, CA152870) and a grant
467 from New York State Stem Cell Science. Lastly, we acknowledge the financial support to
468 J.V. and A.Y. from the National Cancer Institute (#U54 CA143876). The content is solely
469 the responsibility of the authors and does not necessarily represent the official views of
470 the National Cancer Institute or the National Institutes of Health.

471 **References**

- 472 1. Bushue N, Wan YJY (2010) Retinoid pathway and cancer therapeutics. *Adv Drug*
473 *Deliv Rev* 62: 1285-98.
- 474 2. Tang XH, Gudas LJ (2011) Retinoids, retinoic acid receptors, and cancer. *Annu Rev*
475 *Pathol* 6: 345-64.
- 476 3. Cheung FSG, Lovicu FJ, Reichardt JKV (2012) Current progress in using vitamin d
477 and its analogs for cancer prevention and treatment. *Expert Rev Anticancer Ther* 12:
478 811-37.
- 479 4. Nilsson B (1984) Probable in vivo induction of differentiation by retinoic acid of
480 promyelocytes in acute promyelocytic leukaemia. *Br J Haematol* 57: 365-71.
- 481 5. Warrell RP Jr (1993) Retinoid resistance in acute promyelocytic leukemia: new mech-
482 anisms, strategies, and implications. *Blood* 82: 1949-53.
- 483 6. Freemantle SJ, Spinella MJ, Dmitrovsky E (2003) Retinoids in cancer therapy and
484 chemoprevention: promise meets resistance. *Oncogene* 22: 7305-15.
- 485 7. Breitman TR, Selonick SE, Collins SJ (1980) Induction of differentiation of the human
486 promyelocytic leukemia cell line (HL-60) by retinoic acid. *Proc Natl Acad Sci U S A*
487 77: 2936–2940.
- 488 8. Yen A, Roberson MS, Varvayanis S, Lee AT (1998) Retinoic acid induced
489 mitogen-activated protein (MAP)/extracellular signal-regulated kinase (ERK) kinase-
490 dependent MAP kinase activation needed to elicit HL-60 cell differentiation and
491 growth arrest. *Cancer Res* 58: 3163–3172.
- 492 9. Hong HY, Varvayanis S, Yen A (2001) Retinoic acid causes MEK-dependent RAF
493 phosphorylation through RARalpha plus RXR activation in HL-60 cells. *Differentiation*
494 68: 55–66.
- 495 10. Mangelsdorf DJ, Ong ES, Dyck JA, Evans RM (1990) Nuclear receptor that identifies
496 a novel retinoic acid response pathway. *Nature* 345: 224–229.

- 497 11. Congleton J, MacDonald R, Yen A (2012) Src inhibitors, PP2 and dasatinib, increase
498 retinoic acid-induced association of Lyn and c-Raf (S259) and enhance MAPK-
499 dependent differentiation of myeloid leukemia cells. Leukemia 26: 1180-8.
- 500 12. Shen M, Bunaci R, Congleton J, Jensen H, Sayam L, et al. (2011) Interferon regula-
501 tory factor-1 binds c-Cbl, enhances mitogen activated protein kinase signaling and
502 promotes retinoic acid-induced differentiation of HL-60 human myelo-monoblastic
503 leukemia cells. Leuk Lymphoma 52: 2372-9.
- 504 13. Shen M, Yen A (2009) c-Cbl tyrosine kinase-binding domain mutant G306E abolishes
505 the interaction of c-Cbl with CD38 and fails to promote retinoic acid-induced cell dif-
506 ferentiation and G0 arrest. J Biol Chem 284: 25664–25677.
- 507 14. Yen A, Varvayanis S, Smith J, Lamkin T (2006) Retinoic acid induces expression of
508 SLP-76: expression with c-FMS enhances ERK activation and retinoic acid-induced
509 differentiation/G0 arrest of HL-60 cells. Eur J Cell Biol 85: 117–132.
- 510 15. Marchisio M, Bertagnolo V, Colamussi ML, Capitani S, Neri LM (1998) Phosphatidyli-
511 nositol 3-kinase in HL-60 nuclei is bound to the nuclear matrix and increases during
512 granulocytic differentiation. Biochem Biophys Res Commun 253: 346-51.
- 513 16. Congleton J, Jiang H, Malavasi F, Lin H, Yen A (2011) ATRA-induced HL-60 myeloid
514 leukemia cell differentiation depends on the CD38 cytosolic tail needed for membrane
515 localization, but CD38 enzymatic activity is unnecessary. Exp Cell Res 317: 910–
516 919.
- 517 17. Wang J, Yen A (2004) A novel retinoic acid-responsive element regulates retinoic acid
518 induced BLR1 expression. Mol Cell Biol 24: 2423 - 2443.
- 519 18. Yen A (1990) HL-60 cells as a model of growth and differentiation: the significance of
520 variant cells. Hematology Review 4: 5-46.
- 521 19. Yang T, Xiong Q, Enslen H, Davis R, Chow CW (2002) Phosphorylation of NFATc4 by
522 p38 mitogen-activated protein kinases. Mol Cell Biol 22: 3892–3904.

- 523 20. Wang J, Yen A (2008) A MAPK-positive Feedback Mechanism for BLR1 Signaling
524 Propels Retinoic Acid-triggered Differentiation and Cell Cycle Arrest. *J Biol Chem*
525 283: 4375–4386.
- 526 21. Tasseff R, Nayak S, Song S, Yen A, Varner J (2011) Modeling and analysis of retinoic
527 acid induced differentiation of uncommitted precursor cells. *Integr Biol* 3: 578 - 591.
- 528 22. Katagiri K, Hattori S, Nakamura S, Yamamoto T, Yoshida T, et al. (1994) Activation
529 of ras and formation of gap complex during tpa-induced monocytic differentiation of
530 hl-60 cells. *Blood* 84: 1780–1789.
- 531 23. Miranda MB, Johnson DE (2007) Signal transduction pathways that contribute to
532 myeloid differentiation. *Leukemia* 21: 1363–1377.
- 533 24. Hickstein DD, Back AL, Collins SJ (1989) Regulation of expression of the cd11b and
534 cd18 subunits of the neutrophil adherence receptor during human myeloid differenti-
535 ation. *J Biol Chem* 264: 21812–21817.
- 536 25. Hornstein I, Alcover A, Katzav S (2004) Vav proteins, masters of the world of cy-
537 toskeleton organization. *Cell Signal* 16: 1-11.
- 538 26. Song JS, Gomez J, Stancato LF, Rivera J (1996) Association of a p95 vav-containing
539 signaling complex with the fcepsilonlonri gamma chain in the rbl-2h3 mast cell line. ev-
540 idence for a constitutive in vivo association of vav with grb2, raf-1, and erk2 in an
541 active complex. *J Biol Chem* 271: 26962–26970.
- 542 27. Costello PS, Walters AE, Mee PJ, Turner M, Reynolds LF, et al. (1999) The rho-family
543 gtp exchange factor vav is a critical transducer of t cell receptor signals to the calcium,
544 erk, and nf-kappab pathways. *Proc Natl Acad Sci U S A* 96: 3035–3040.
- 545 28. Graham D, Robertson C, Bautista J, Mascarenhas F, Diacovo M, et al. (2007)
546 Neutrophil-mediated oxidative burst and host defense are controlled by a Vav-
547 PLCgamma2 signaling axis in mice. *J Clin Invest* 117: 3445–3452.
- 548 29. Cleghon V, Morrison DK (1994) Raf-1 interacts with fyn and src in a non-

- 549 phosphotyrosine-dependent manner. *J Biol Chem* 269: 17749–17755.
- 550 30. Zimmermann S, Moelling K (1999) Phosphorylation and regulation of raf by akt (pro-
551 tein kinase b). *Science* 286: 1741–1744.
- 552 31. Ritt DA, Zhou M, Conrads TP, Veenstra TD, Copeland TD, et al. (2007) Ck2 is a
553 component of the ksr1 scaffold complex that contributes to raf kinase activation. *Curr
554 Biol* 17: 179–184.
- 555 32. Hekman M, Wiese S, Metz R, Albert S, Troppmair J, et al. (2004) Dynamic changes in
556 c-raf phosphorylation and 14-3-3 protein binding in response to growth factor stimula-
557 tion: differential roles of 14-3-3 protein binding sites. *J Biol Chem* 279: 14074–14086.
- 558 33. Dhillon AS, Yip YY, Grindlay GJ, Pakay JL, Dangers M, et al. (2009) The c-terminus
559 of raf-1 acts as a 14-3-3-dependent activation switch. *Cell Signal* 21: 1645–1651.
- 560 34. Kim HS, Lim IK (2009) Phosphorylated extracellular signal-regulated protein kinases
561 1 and 2 phosphorylate sp1 on serine 59 and regulate cellular senescence via tran-
562 scription of p21sdi1/cip1/waf1. *J Biol Chem* 284: 15475–15486.
- 563 35. Milanini-Mongiat J, Pouyss?gur J, Pag?as G (2002) Identification of two sp1 phospho-
564 rylation sites for p42/p44 mitogen-activated protein kinases: their implication in vas-
565 cular endothelial growth factor gene transcription. *J Biol Chem* 277: 20631–20639.
- 566 36. Zhang Y, Cho YY, Petersen BL, Zhu F, Dong Z (2004) Evidence of stat1 phospho-
567 lation modulated by mapks, mek1 and msk1. *Carcinogenesis* 25: 1165–1175.
- 568 37. Li Z, Theus MH, Wei L (2006) Role of erk 1/2 signaling in neuronal differentiation of
569 cultured embryonic stem cells. *Dev Growth Differ* 48: 513–523.
- 570 38. Yen A, Reece SL, Albright KL (1984) Dependence of hl-60 myeloid cell differentiation
571 on continuous and split retinoic acid exposures: precommitment memory associated
572 with altered nuclear structure. *J Cell Physiol* 118: 277–286.
- 573 39. Ferrell J (2002) Self-perpetuating states in signal transduction: positive feedback,
574 double-negative feedback and bistability. *Curr Opin Cell Biol* 14: 140-8.

- 575 40. Xiong W, Ferrell J (2003) A positive-feedback-based bistable 'memory module' that
576 governs a cell fate decision. *Nature* 426: 460-5.
- 577 41. Bagci EZ, Vodovotz Y, Billiar TR, Ermentrout GB, Bahar I (2006) Bistability in apop-
578 tosis: roles of bax, bcl-2, and mitochondrial permeability transition pores. *Biophys J*
579 90: 1546-59.
- 580 42. Luan D, Zai M, Varner JD (2007) Computationally derived points of fragility of a human
581 cascade are consistent with current therapeutic strategies. *PLoS Comput Biol* 3:
582 e142.
- 583 43. Wayman JA, Sagar A, Varner JD (2015) Dynamic modeling of cell-free biochemical
584 networks using effective kinetic models. *Processes* 3: 138.
- 585 44. Milo R, Jorgensen P, Moran U, Weber G, Springer M (2010) Bionumbers—the
586 database of key numbers in molecular and cell biology. *Nucleic Acids Res* 38: D750-
587 3.
- 588 45. Bezanson J, Edelman A, Karpinski S, Shah VB (2014) Julia: A fresh approach to
589 numerical computing. *CoRR* abs/1411.1607.
- 590 46. Hindmarsh A, Brown P, Grant K, Lee S, Serban R, et al. (2005) Sundials: Suite of non-
591 linear and differential/algebraic equation solvers. *ACM Transactions on Mathematical
592 Software* 31: 363-396.
- 593 47. Brooks SC, Kazmer S, Levin AA, Yen A (1996) Myeloid differentiation and retinoblas-
594 toma phosphorylation changes in HL-60 cells induced by retinoic acid receptor- and
595 retinoid X receptor-selective retinoic acid analogs. *Blood* 87: 227–237.
- 596 48. Jensen HA, Yourish HB, Bunaciu RP, Varner JD, Yen A (2015) Induced myelomono-
597 cytic differentiation in leukemia cells is accompanied by noncanonical transcription
598 factor expression. *FEBS Open Bio* 5: 789-800.

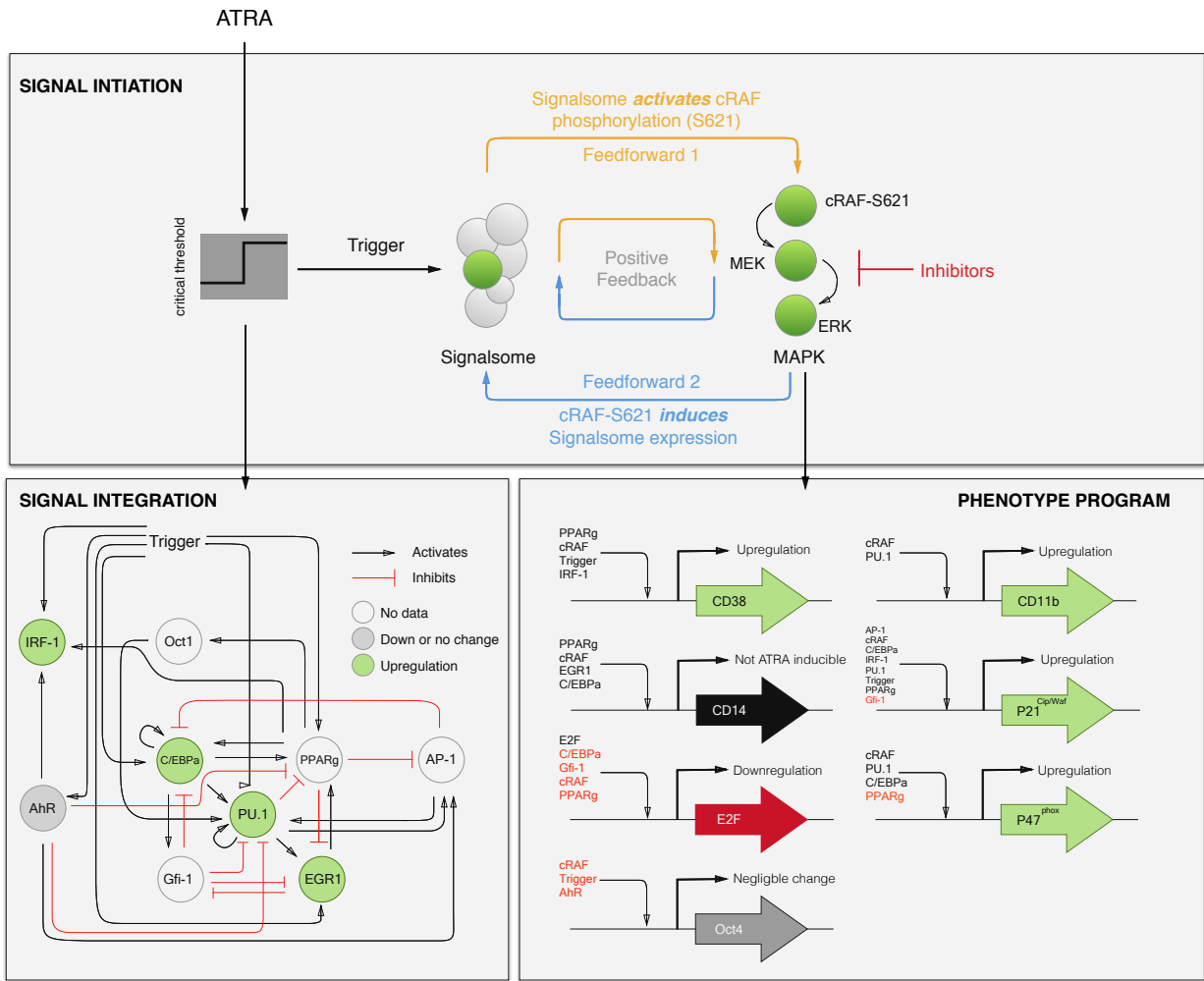


Fig. 1: Schematic of the effective ATRA differentiation circuit. Above a critical threshold, ATRA activates an upstream Trigger, which induces signalsome complex formation. Signalsome activates the mitogen-activated protein kinase (MAPK) cascade which in turn drives the differentiation program and signalsome formation. Both Trigger and activated cRaf-S621 drive a phenotype gene expression program responsible for differentiation. Trigger activates the expression of a series of transcription factors which in combination with cRaf-S621 result in phenotypic change.

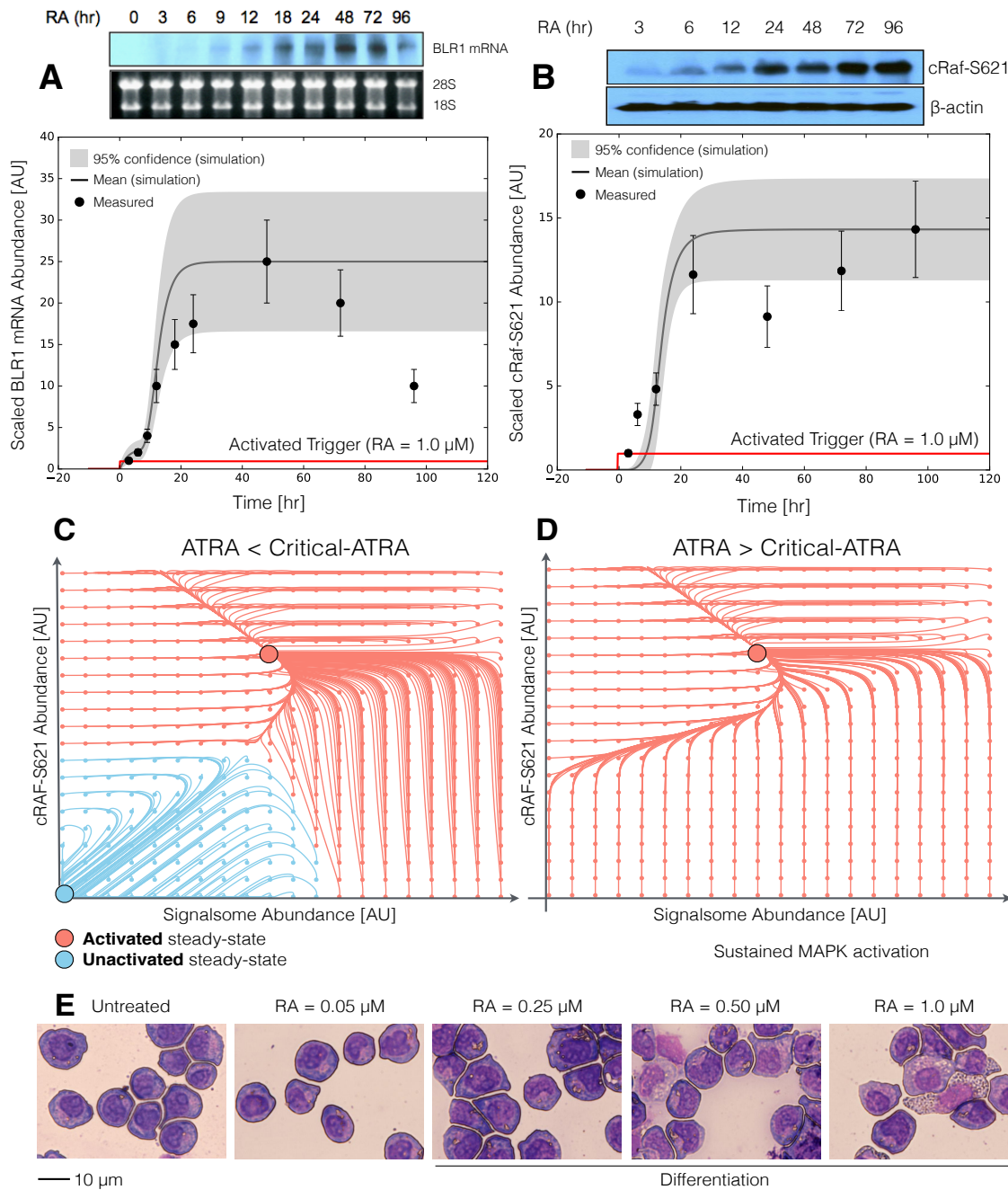


Fig. 2: Model analysis for ATRA-induced HL-60 differentiation. A: BLR1 mRNA versus time following exposure to $1\mu\text{M}$ ATRA at $t = 0$ hr. B: cRaf-pS621 versus time following exposure to $1\mu\text{M}$ ATRA at $t = 0$ hr. Points denote experimental measurements, solid lines denote the mean model performance. Shaded regions denote the 99% confidence interval calculated over the parameter ensemble. C: Signalsome and cRaf-pS621 nullclines for ATRA below the critical threshold. The model had two stable steady states and a single unstable state in this regime. D: Signalsome and cRaf-pS621 nullclines for ATRA above the critical threshold. In this regime the model had only a single stable steady state. E: Morphology of HL-60 as a function of ATRA concentration ($t = 72$ hr).

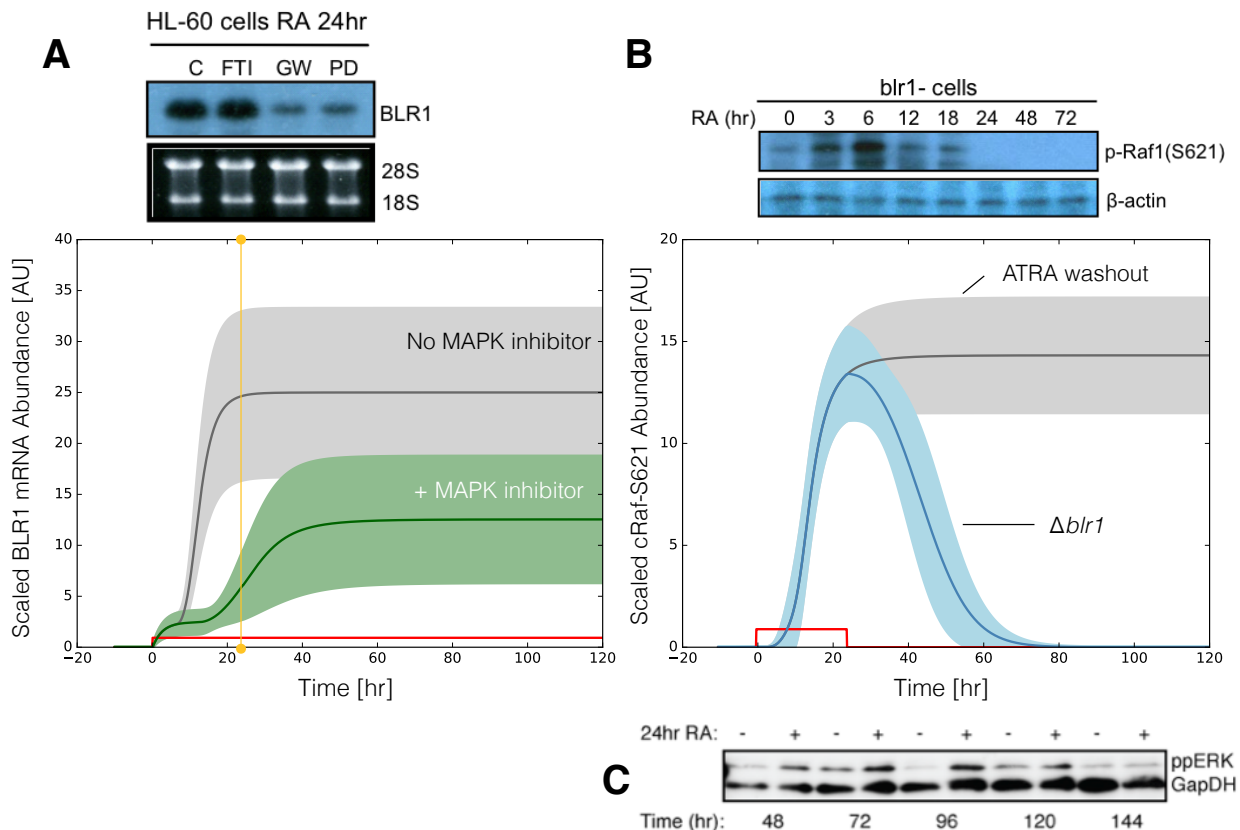


Fig. 3: Model simulation following exposure to $1\mu\text{M}$ ATRA. A: BLR1 mRNA versus time with and without MAPK inhibitor. B: cRaf-pS621 versus time following pulsed exposure to $1\mu\text{M}$ ATRA with and without BLR1. Solid lines denote the mean model performance, while shaded regions denote the 99% confidence interval calculated over the parameter ensemble. C: Western blot analysis of phosphorylated ERK1/2 in ATRA washout experiments. Experimental data in panels A and B were reproduced from Wang and Yen (20), data in panel C is reported in this study.

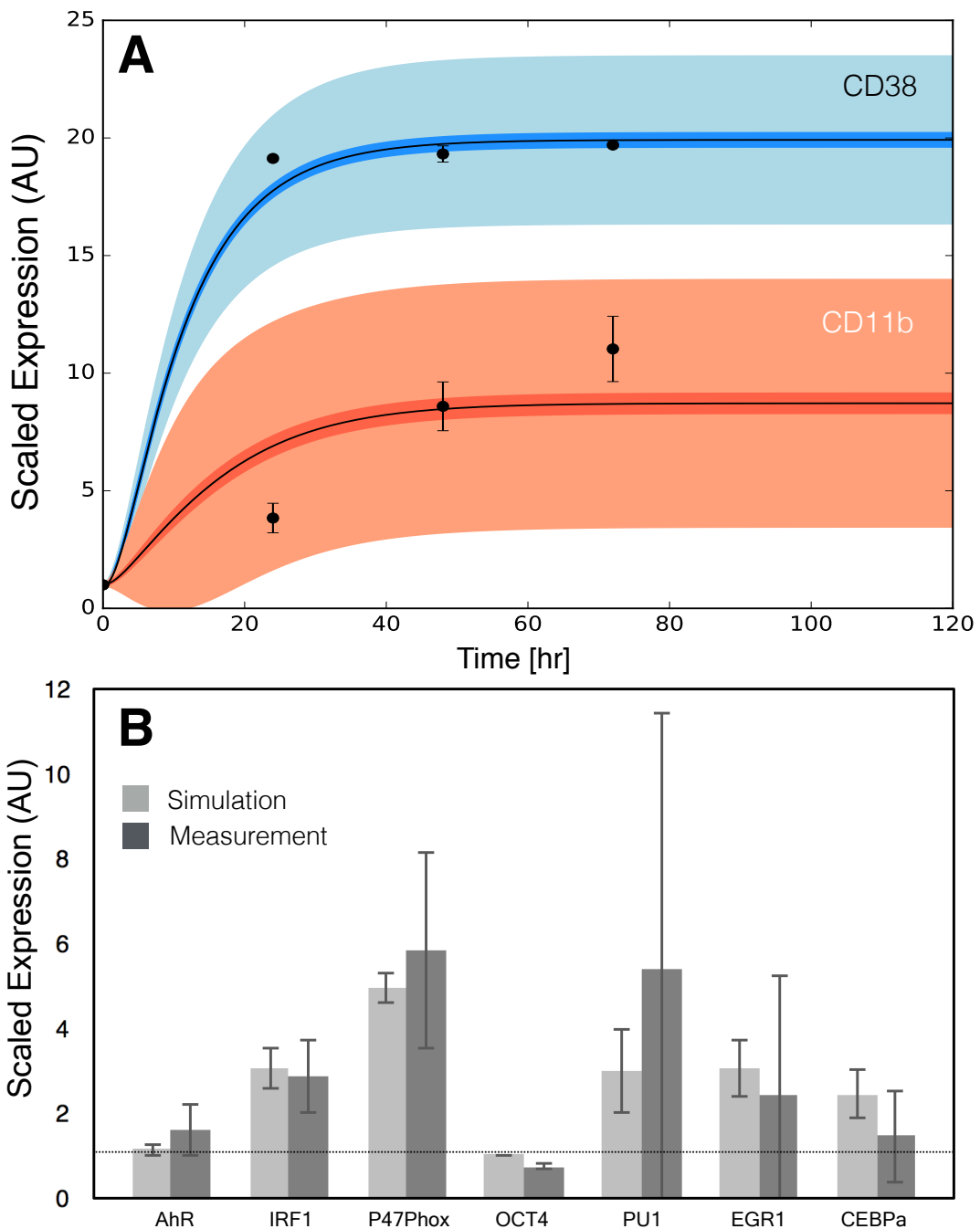


Fig. 4: Model simulation of the HL-60 gene expression program following exposure to $1\mu\text{M}$ ATRA at $t = 0$ hr. A: CD38 and CD11b expression versus time following ATRA exposure at time $t = 0$ hr. B: Gene expression at $t = 48$ hr following ATRA exposure. Experimental data in panels A and B were reproduced from Jensen et al. (48).

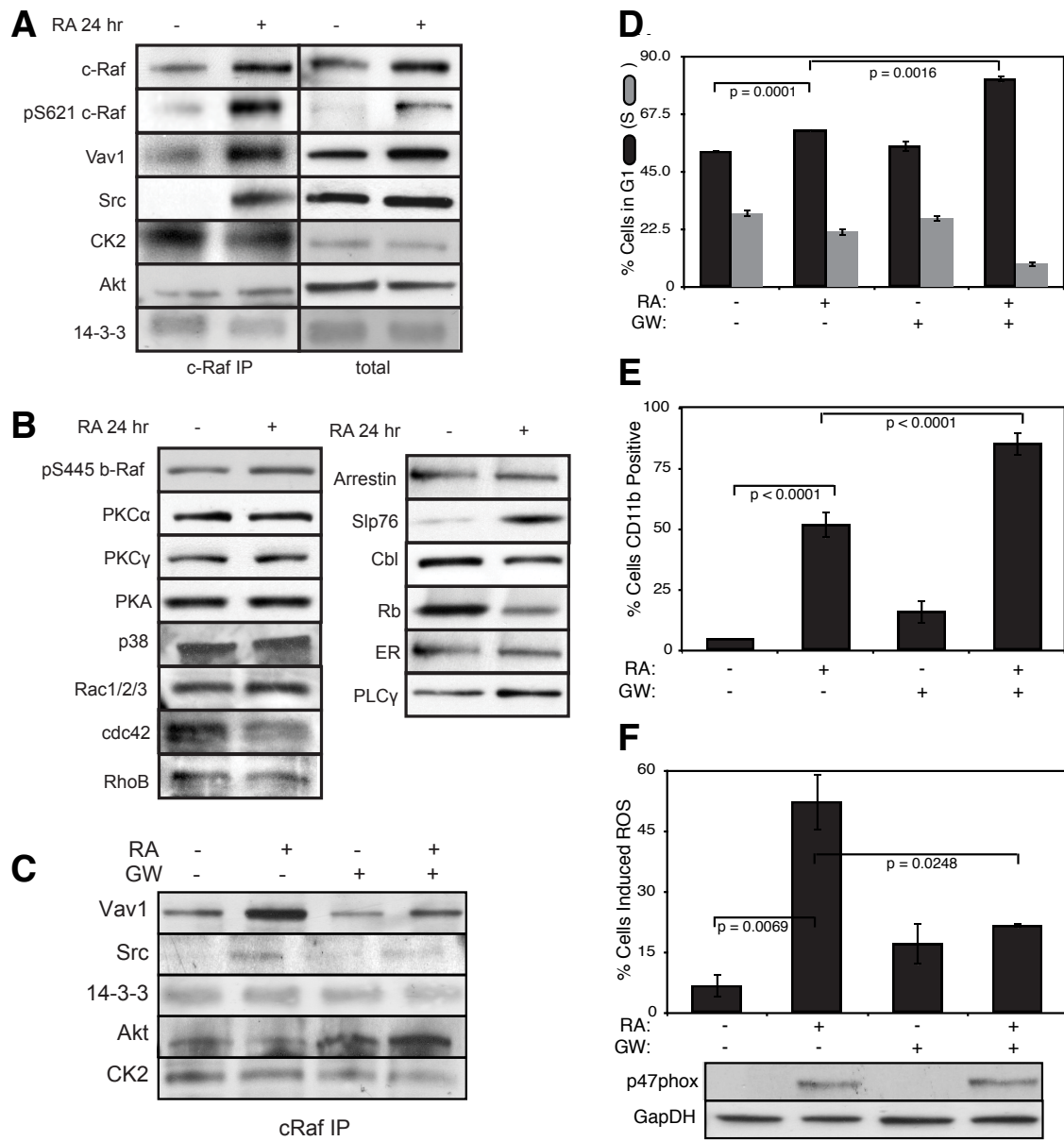


Fig. 5: Investigation of a panel of possible Raf interaction partners in the presence and absence of ATRA. A: Species identified to precipitate out with Raf: first column shows Western blot analysis on total Raf immunoprecipitation with and without 24 hr ATRA treatment and the second on total lysate. B: The expression of species considered that did not precipitate out with Raf at levels detectable by Western blot analysis on total lysate. C: Effect of the Raf inhibitor GW5074 on Raf interactions as determined by Western blot analysis of total Raf immunoprecipitation. The Authors note the signal associated with Src was found to be weak. D: Cell Cycle distribution as determined by flow cytometry indicated arrest induced by ATRA, which was increased by the addition of GW5074. E: Expression of the cell surface marker CD11b as determined by flow cytometry indicated increased expression induced by ATRA, which was enhanced by the addition of GW5074. F: Inducible reactive oxygen species (ROS) as determined by DCF flow cytometry. The functional differentiation response of ATRA treated cells was mitigated by GW5074.